# Structural behaviour of tunnels exposed to fire using numerical modelling strategies

Díaz, Rafael Sanabria; Lantsoght, Eva; Hendriks, Max A.N.

**DOI**
10.1016/j.firesaf.2024.104335

**Publication date**
2025

**Document Version**
Final published version

**Published in**
Fire Safety Journal

Fire Safety Journal 152 (2025) 104335

Contents lists available at ScienceDirect

Fire Safety Journal

journal homepage: www.elsevier.com/locate/firesaf

# Structural behaviour of tunnels exposed to fire using numerical modelling strategies

Rafael Sanabria Díaz [a,*], Eva Lantsoght [a,b], Max A.N. Hendriks [a,c]

[a] Delft University of Technology, Delft, The Netherlands
[b] Universidad San Francisco de Quito, Quito, Ecuador
[c] Norwegian University of Science and Technology, Trondheim, Norway

ARTICLE INFO

Dataset link: https://gitlab.tudelft.nl/rsanabriadiaz/brandwerendheid-landtunnels

*Keywords:*
Fire
Reinforced concrete
Thermal analysis
Finite element method
Nonlinear analysis
Tunnels

ABSTRACT

Despite the low probability of occurrence, fire events are a major hazard for structures, which can lead to severe socio-economic impact. Although reinforced concrete (RC) tunnels are an important component in transportation infrastructure, their structural behaviour under high temperatures is not yet fully understood. This study investigates the thermo-mechanical response of tunnels subjected to fire using nonlinear finite element analysis (NLFEA). For this purpose, recent experimental tests of large-scale reinforced concrete tunnels with and without fire protection are simulated. Different modelling strategies are discussed, and a detailed description of the constitutive model employed is presented. Then, model-to-model and model-to-experiment comparisons are conducted to identify the advantages and limitations of each approach. The analyses demonstrate the relevance of proper spalling modelling on the tunnel's temperature distribution. The models also show a good agreement with the experimentally observed damage patterns. Finally, recommendations regarding modelling choices and further research topics are discussed.

## 1. Introduction

The behaviour of reinforced concrete (RC) tunnel linings exposed to fire is an issue of significant importance for the safe operation of transportation infrastructure. Due to the enclosed geometry and confined space, tunnel fires can develop rapidly with gas temperatures rising to more than 1000 °C, leading to more intensive fires in comparison with building compartments. As a result, tunnel fires may lead to severe consequences, including loss of human lives, structural damage and socioeconomic impact due to prolonged traffic disruptions [1]. Given the constant increment of heavy goods vehicles and ion-battery electric vehicles, the fire response of tunnels has received considerable attention over the last years. Important research has been done regarding evacuation strategies, fire dynamics, and smoke simulations to mitigate the consequences of fire in tunnels. However, fewer studies have focused on areas such as structural assessment, damage quantification, and robustness of RC tunnels [2].

The current practice for the design of RC structures exposed to fire is predominantly based on a prescriptive approach. EN 1992-1-2:2004 [3] includes tabulated methods to estimate minimum cross-section values and reinforcement cover. These values are derived from experimental data of single elements or sub-assemblies, field experience and numerical simulations. The tabulated methods generally provide a conservative estimate; therefore, more precise approaches can be applied, such the 500 °C isotherm method. This method consists of reducing the cross-section of the structural element up to the damaged layer in which the temperatures reach more than 500 °C. The rest of the concrete cross-section is considered fully effective, maintaining its values of compressive strength and elastic modulus from ambient temperature. The material properties of the reinforcing steel are considered according to the actual temperatures provided by the thermal analysis.

Despite the simplifications assumed in traditional prescriptive methods, the safety performance of RC structures subjected to elevated temperatures is achieved in most cases, even without using any additional protective measures, owing to non-combustibility and low thermal conductivity of concrete. However, in complex structures such as tunnel linings, more sophisticated methods are generally required to guarantee structural integrity and to ensure a sufficient residual capacity to sustain the fire effects without collapsing. In this case, using of performance-based design (PBD) represents an alternative in engineering practice. Instead of using step-by-step design regulations, PBD strategies rely on the explicit definition of performance objectives and the demonstration that these objectives are fulfilled by design. In the case of fire engineering, the performance objectives are predominantly

* Corresponding author.
*E-mail address:* r.a.sanabriadiaz@tudelft.nl (R.S. Díaz).

https://doi.org/10.1016/j.firesaf.2024.104335
Received 29 August 2024; Received in revised form 26 November 2024; Accepted 19 December 2024
Available online 26 December 2024

based on the acceptable level of consequence during a specified period in a fire event [4].

In most cases, the application of PBD requires the use of advanced analysis methods to demonstrate that the defined performance can be achieved. In particular, the numerical simulation of RC structures combines multiple challenges, including cracking, degradation of material properties, thermal dilatation, and yielding of the reinforcement, among others. Additional complex phenomena, such as spalling, may also rise, reducing the structure safety level. Concrete spalling is characterised by the breaking off of layers from the heated concrete surface, usually in an explosive and sudden manner [5,6]. The spalling process of concrete subjected to elevated temperatures is not fully understood. Therefore, it is recommendable to consider all unprotected concrete prone to spalling [7]. The described challenges, and the uncertainties associated with them, have hindered the wide use of PBD in RC structures.

In the case of tunnels, different studies can be found in the literature regarding the application of nonlinear finite element analysis (NLFEA) for the simulation of tunnel cross-sections or tunnel sub-components. The simplest approaches relies on using 2D beam finite element analysis [8–10]. More sophisticated approaches have also been applied based on 2D continuum [11–13] and shell elements [14,15]. The use of fully 3D solid elements has been limited to the simulation of tunnel sub-components [15,16]. In summary, these studies highlight the potential of using advanced numerical models for fire design and research but also point out the influence of structural modelling choices on the results obtained from the simulations.

In this context, this study investigates and compares different strategies regarding the modelling of tunnels exposed to fire using NLFEA. The proposed strategies are broadly explained, including a description of the material constitutive model. The numerical analyses were validated on the basis of large fire tests of tunnel segments reported in the literature. The experimental and the different numerical strategies are compared in terms of temperature distribution, deflections, crack patterns and bending moment redistribution. Finally, key outcomes and conclusions are derived about the capabilities and limitations of the simulations and the feasibility of using finite element-based analyses in the design and post-fire assessment of tunnels.

## 2. Constitutive models for reinforced concrete at elevated temperatures

### 2.1. Overview

Concrete behaviour at elevated temperatures is highly nonlinear due to the combinations of different phenomena, including thermal, chemical, hygral, and mechanical processes. As a result, concrete undergoes thermal expansion and strength degradation. In the past decades, several constitutive material approaches have been developed in the context of meso- and macro-scale models to simulate concrete at elevated temperatures. Meso-scale models, considering the heterogeneity of concrete, have been used to study the fracture process of heated concrete and explosive spalling mechanism [5,17,18]. These constitutive models have been implemented using finite element method (FEM), discrete element method (DEM), and lattice models. On the other hand, macro-models have been applied to study the global thermo-mechanical behaviour of reinforced concrete members predominately using FEM with a reasonably low computational cost in comparison with meso-scale models [8,13,16,19–24]. Therefore, this study emphasises the application of macro-scale models for the investigation of tunnels exposed to fire.

### 2.2. Total strain formulation

In the context of continuum models based on elasticity and elasto-plastic behaviour, a common assumption is to decompose the total strain in concrete subjected to fire as follows :

$$\varepsilon_{tot} = \varepsilon_{th} + \varepsilon_{\sigma} + \varepsilon_{tr} + \varepsilon_{cr} \tag{1}$$

where $\varepsilon_{th}$, $\varepsilon_{\sigma}$, $\varepsilon_{tr}$ and $\varepsilon_{cr}$ are the free thermal strain, mechanical strain, transient creep strain and basic creep strain. For design verification purposes, the basic creep strain is generally omitted owing to the relatively short period of a fire event [25]. The free thermal strain is governed by the thermal expansion coefficient, and it is associated with the thermal expansion of concrete. The rate of the free thermal strain is given by:

$$\dot{\varepsilon}_{th} = \alpha\dot{\theta} \tag{2}$$

where $\alpha$ is thermal expansion coefficient and $\dot{\theta}$ is the temperature rate. According to EN 1992-1-2:2004 [3], the thermal expansion coefficient is defined as temperature- and aggregate-dependent.

The transient creep strain is an additional strain that develops during the first-time heating of concrete subjected to initial stress. Experimental tests show that concrete specimens under loading exhibit smaller thermal expansion than a stress-free heating specimen [26,27]. Transient creep strain is sometimes referred to as load-induced thermal strain (LITS), although some researchers interpret transient creep strain to be only one component of LITS [28]. In constitutive models, transient creep can be considered using implicit or explicit formulations. In the former one, the stress is directly related to the mechanical strain without calculating the transient strain. The transient creep is modelled indirectly by shifting the strain at maximum stress. This simplification is adopted in several models in the literature, including the EN 1992-1-2:2004 [3] model. In contrast, in explicit models, the thermal strain is accounted for based on the applied stress and temperature [29]. In explicit models, the transient creep strain is computed explicitly, and it is considered to be irrecoverable during the unloading and/or cooling phase (the period after a fire in which the structure temperature is cold down).

### 2.3. Temperature-dependent material properties

The material properties of concrete and reinforcing steel are strongly dependent on temperature. The relationships recommended in EN 1992-1-2:2004 [3] were included in the numerical models carried out in this study. Some additional parameters, such as the concrete fracture energy, were derived from previous works [16]. It should be noted that in macro-scale modelling approaches, neither the moisture transport nor the dehydration chemical processes in heated concrete are modelled explicitly. It is assumed that the effect of those processes is described on a macroscopic scale through the temperature-dependent material behaviour. In addition to the mechanical properties, thermal properties are also used for the thermal analysis. The thermal conductivity and the volumetric specific heat are also defined according to EN 1992-1-2:2004 [3]. These input parameters are defined to be temperature-dependent and irreversible during the cooling phase. An average value between the lower and upper bound limits prescribed by EN 1992-1-2:2004 [3] is used for the thermal conductivity.

## 3. Case study: fire tests of large-scale HZMB tunnel segments

The tests performed by Duan et al. [30], Dong et al. [31] and Lin et al. [32] are used as a reference in this study for comparison with the numerical simulations. The experiments represented a reduced scale (1:5) model of an immersed tunnel segment of the Hong Kong-Zhuhai-Macao Bridge (HZMB) project. The cross-section of the tunnel is visualised in Fig. 1(a), and the main parameters of the considered fire scenarios are summarised in Table 1. The tunnel segments were cast with a C50 concrete mix with siliceous aggregate with a measured compressive strength of 60 MPa and moisture content of 5.1%. The rebar yield strength was estimated at 442.3 MPa. The protective coating applied in the scenario tested by Duan etl al. [30] consisted of three

**Table 1**
Fire scenarios considered in the large-scale tunnel segment experiments.

| Fire scenario | Number of tubes exposed to fire | Fire protection | Maximum temperature [°C] | Duration of heating phase [min] | Concrete spalling |
|---|---|---|---|---|---|
| Duan et al. [30] | 1 | Yes | 1113.7 | 365 | No |
| Dong et al. [31] | 2 | No | 1344.8 | 245 | Yes |
| Lin et al. [32] | 1 | No | 1304.0 | 202 | Yes |

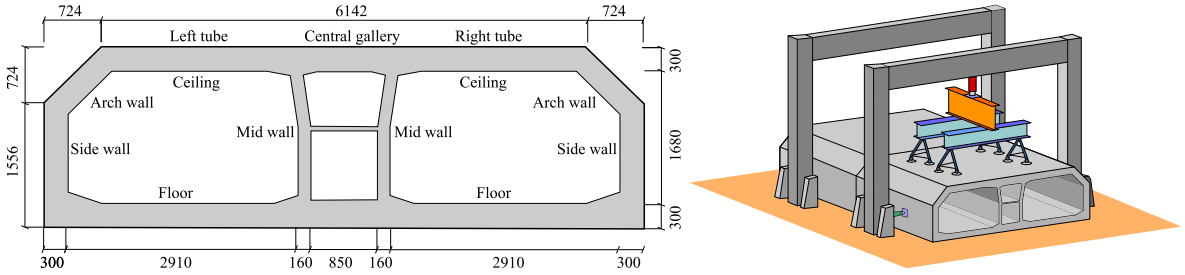


(a) Cross-section (measures in mm) (b) Experimental setup

**Fig. 1.** Cross-section and setup of the tunnel segment fire test.
*Source:* Adapted from [31].

layers of coating sprayed on a wire mesh fixed to the inner surface of the tunnel. The total thickness of the coating was 30 mm, and the main components were expanded perlite, expanded vermiculite, and composite Portland cement.

During the test executions, vertical and horizontal outer loads were applied before introducing of the thermal gradient using the setup illustrated in Fig. 1(b). The tunnel segments were subjected to a total vertical load of 2427.4 kN and a horizontal load of 437.2 kN on both side walls. These loads aimed to represent the service loads from the sediment and seawater. The load was maintained constant during the fire event (both heating and cooling phases). The tunnel tubes, enclosed by brick walls at each end, were used as furnace chambers for the controlled application of the fire scenarios. The heating system used in the tests consisted of oil burners. During the tests, temperatures, deformations, cracking, and concrete spalling were measured. The temperature in the concrete was recorded using type-K thermocouples at different locations and depths. In addition to thermocouples, infrared thermography was used to measure the temperature of the outer surface of the tunnel. An acoustic emission system was employed to record the spalling and cracking behaviour of the tunnel during the test. Furthermore, the deformation of the tunnel was measured by LVDTs and inclinometers.

At the end of the tests, it was found that the capacity of the three tunnel segments was sufficient to withstand the applied thermal load (during the heating and cooling phases). However, damage on the heated and unheated sides of the tunnel segments was observed in all the experiments. In the test conducted by Duan et al. [30], the fire-resistive coating performed well, and concrete spalling did not occur, but concrete cracking was noticed in the tunnel's unheated side and even in the mid gallery and the left tube that was not exposed to fire. More severe damage was observed in the fire scenarios without fire protection. Dong et al. [31] and Lin et al. [32] reported that almost 100% of the exposed fire concrete surface was affected by spalling. As a consequence, the diameter of the exposed rebars was reduced, and in some locations, the rebars were fully melted.

## 4. Modelling strategies

### 4.1. Overview

In this study, two different modelling approaches were employed to represent the thermo-mechanical behaviour of the three tunnels experiments described in the previous section. An overview of the main characteristics of each strategy is presented in Table 2. Both strategies are based on nonlinear finite element analysis using the total strain formulation outlined in Section 2.2. For simplicity and computation time, the analyses are limited to a 2D model representation. The numerical models based on Strategy I were developed using the commercially available software SAFIR [33]. In this approach, the tunnel structure is modelled using 2D beam finite elements. On the other hand, the Strategy II made use of 2D continuum finite elements using the software DIANA [34]. Additional aspects of both strategies are discussed in the following items.

### 4.2. Constitutive material models considerations

The general aspects for modelling reinforced concrete at elevated temperatures presented in Sections 2.2 and 2.3 are implemented in both strategies investigated in this study. Therefore, the degradation of concrete and reinforcing steel due to temperature and their thermal properties are based on the relationships found in EN 1992-1-2:2004 [3]. In the constitutive model used in DIANA (Strategy II), the concrete nonlinear behaviour is defined by the total strain fixed crack model. This model represents the cracking damage based on the stiffness reduction at the integration points using multi-axial stress–strain relationships. After cracking, the concrete tension softening is represented by the fracture energy model proposed by [35]. In compression, the concrete is represented by the parabolic stress–strain [36] curve and accounts for the possible increment in strength and ductility due to confinement effects based on the model proposed by [37]. Moreover, the reduction of compressive strength due to cracking perpendicular to the compressive direction is also included using the model proposed by [38]. The constitutive model implemented in SAFIR (Strategy I) for beam elements is based on uniaxial stress–strain relationships using a plastic-damage formulation. In compression, the concrete behaviour has an elastic and hardening branch (using the same expression in EN 1992-1-2:2004 [3]) followed by a softening branch until failure. The concrete tensile strength is omitted in the numerical analyses carried out in this study.

The main differences between the strategies' constitutive models are related to modelling transient creep strain and the behaviour during the cooling phase. In SAFIR, the constitutive model adopts an explicit transient creep strain according to [29]. DIANA adopts an implicit model using the EN 1992-1-2:2004 [3] formulation. The latter simplification does not account for the transient strain creep irreversibility during the cooling phase. The SAFIR constitutive model accounts for

**Table 2**
Comparison of modelling strategies proposed in this study.

| General aspects | Strategy I | Strategy II |
|---|---|---|
| Software | SAFIR (version 2022) | DIANA (version 10.8) |
| Element type | 2D beam elements for mechanical analysis 2D plane elements for thermal analysis at each cross-section | 2D Continuum element with plane stress/strain idealisation and in-plane heat flow |
| Analysis type | Staggered analysis:<br>1. Thermal analysis<br>2. Mechanical analysis with superposition of thermal effects | Staggered analysis:<br>1. Thermal analysis<br>2. Mechanical analysis with superposition of thermal effects |
| Thermal analysis | | |
| Specific heat and thermal conductivity | Conform EN 1992-1-2:2004 | Conform EN 1992-1-2:2004 |
| Mechanical analysis | | |
| Concrete mechanical model | Plastic damage approach | Total strain fixed crack model (smeared crack approach) |
| Reinforcement properties | Elastic-perfectly plastic behaviour | Elastic-perfectly plastic behaviour |
| Material degradation model during heating phase | Conform EN 1992-1-2:2004 | Conform EN 1992-1-2:2004 and additional relationships for specific parameters |
| Transient creep strain | Explicit model | Implicit model |

additional material degradation during the cooling phase based on the maximum temperature reached by the material. SAFIR considers that the concrete loses an additional 10% of strength in accordance with EN 1994-1-2:2005 [39] recommendations. Furthermore, a residual thermal expansion is considered when the concrete returns to ambient temperature based on the experimental tests by [26]. The constitutive model adopted in DIANA assumes that damage recovery due to cracking is not possible. However, a full recovery of the thermal strains is possible during the cooling phase. In the case of reinforcing steel, preliminary simulations in DIANA indicated unrealistic results with a full recovery of the reinforcing steel mechanical properties upon cooling, even after reaching temperatures higher than 1000 °C. Therefore, a FORTRAN user-supplied subroutine was implemented to restrict the yield strength and the Young modulus values based on the maximum temperature reached during the heating phase.

### 4.3. Staggered analysis procedure

Both strategies perform a staggered procedure to couple the thermal and the mechanical analyses. First, the temperature in the structure is computed using a nonlinear transient thermal analysis. Then, a nonlinear structural analysis is executed to account for the material degradation due to temperatures and thermal strains (obtained in the proceeding thermal analysis). The main assumption of this approach is that the temperature distribution is independent of the mechanical response. The regular Newton–Raphson is employed to achieve the equilibrium in the iterative procedure. In both software, the increments are updated with a cutback-based automatic incremental procedure. This algorithm reduces the number of steps required to apply the total time (i.e., the fire duration) and automatically decreases the time increments to recover from non-convergence steps in the iterative procedure. The method is summarised as follows:

$$ {}^{t+\Delta t}\lambda_{\min} \leq {}^{t+\Delta t}\lambda \leq {}^{t+\Delta t}\lambda_{\max} \tag{3} $$

where ${}^{t+\Delta t}\lambda_{\min}$ and ${}^{t+\Delta t}\lambda_{\max}$ are the desired minimum and maximum time steps, and ${}^{t+\Delta t}\lambda$ is the time step of the new time increment. First, the maximum time step size is applied in a single step. If the iterative procedure fails to converge, the load step is decreased by a cutback factor. If, after successive failures, the load step becomes smaller than the minimum specified time step, the analysis stops. For the simulations, in DIANA, a maximum time step of 10 min was used, while a maximum time step of 8 s was adopted in SAFIR to avoid convergence issues. For both strategies, the computation time was similar. As an example, the numerical models for the 480-min fire test conducted by Duan et al. [30] lasted 69 and 58 min for the strategies I and II, respectively (12th Gen Intel Core i7 1.80 GHz).

### 4.4. Mesh discretisation and boundary conditions

As mentioned, a key difference between the proposed strategies was the finite element type used to obtain the mechanical response. In Strategy I, the tunnel was represented using 2D finite beam elements, as illustrated in Fig. 2(a). The mesh consisted of three-node elements based on Euler–Bernoulli beam theory with two Gauss points along in the longitudinal direction. An average mesh size of 100 mm was used for the structural analysis. Different segments were created depending on the geometry and longitudinal rebar amount of each cross-section. In the thermal analysis, these sections were represented with 2D quadrilateral finite elements using the boundary conditions detailed in Fig. 2(a). The temperature distribution calculated on these elements is transferred to the beam elements. An average mesh size of 30 mm was used for the 2D quadrilateral elements. This mesh size was found to be sufficient to capture the nonlinear thermal gradient at the concrete cover.

In Strategy II, the tunnel was discretised using 2D continuum elements as shown in Fig. 2(b). Within this approach, two different modelling assumptions were compared: plane stress and plane strain idealisations. The former approach implies that the out-of-plane stresses are zero, whereas in the latter one, it is assumed that there is no out-of-plane displacement. For the staggered analysis, first-order isoparametric quadrilateral elements (denoted in DIANA as Q4HT) are employed for the thermal calculations. In the subsequent mechanical analysis, these elements were automatically upgraded to second-order isoparametric elements denoted as CQ16M (for plane stress) and CQ16E (for plane strain). An average mesh size of 30 mm was adopted in the analyses. As indicated in Fig. 2(b), the DIANA models included the representation of longitudinal and shear reinforcement. The rebars were represented by truss elements embedded in the concrete elements.

For the transient thermal analysis, the recorded furnace temperatures reported in the experimental tests were used as an input in both strategies. Heat transfer was considered through convection and radiation mechanisms. Convection coefficients at the exposed and unexposed sides were considered as 50 W/m$^2$ °C and 4 W/m$^2$ °C, respectively, as recommended in [40]. An emissivity coefficient of 0.7 for the radiation thermal transfer is used. The fire coating was modelled considering a thermal conductivity of 0.125 W/(m °C) and thermal capacity of 52 500 J/(m$^3$ °C). These properties were derived from the coating components reported by Duan et al. [30] and were assumed constant during the fire. The stiffness provided by the coating layer was neglected in the mechanical analysis. The interaction between the tunnel segments and the foundation was modelled using spring (SAFIR) and interface elements (DIANA) with no tension and a high compression bedding stiffness (75

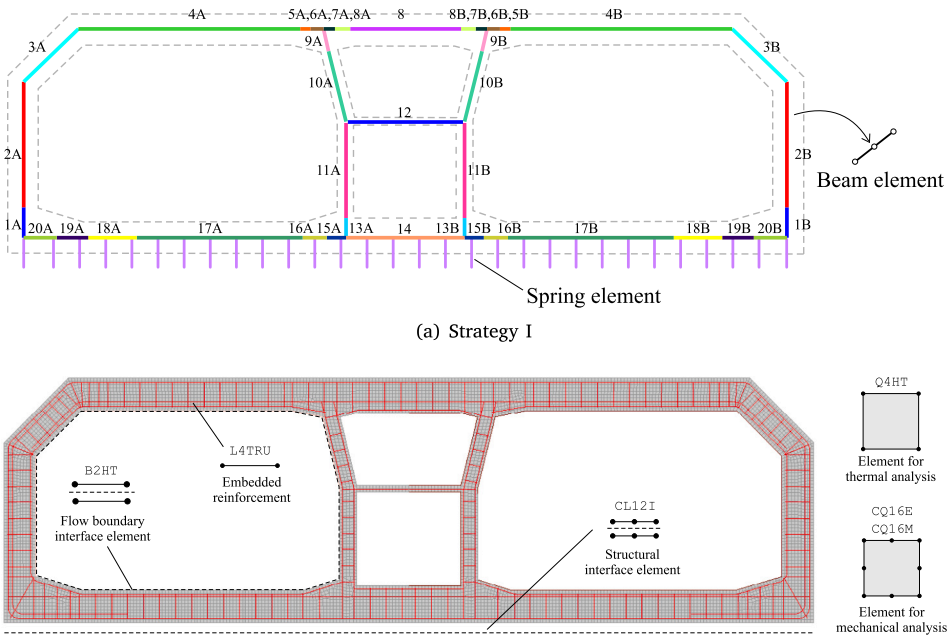


**Fig. 2.** Typical mesh used in the numerical analysis for each strategy.

**Table 3**
Overview of numerical analyses conducted for each fire scenario and modelling strategy.

| Fire scenario | Strategy I | Strategy II |
|---|---|---|
| A: Fire in one tube with coating (no spalling), Duan et al. [30] | 1. Beam elements | 6. Plane stress elements<br>7. Plane strain elements |
| B: Fire in both tubes without coating Dong et al. [31] | Without spalling:<br>2. Beam elements<br><br>With spalling:<br>3. Beam elements | Without spalling:<br>8. Plane stress elements<br>9. Plane strain elements<br>With spalling:<br>10. Plane stress elements<br>11. Plane strain elements |
| C: Fire in one tube without coating Lin et al. [32] | Without spalling:<br>4. Beam elements<br><br>With spalling:<br>5. Beam elements | Without spalling:<br>12. Plane stress elements<br>13. Plane strain elements<br>With spalling:<br>14. Plane stress elements<br>15. Plane strain elements |

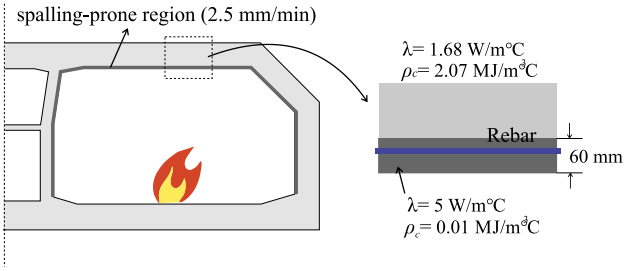


**Fig. 3.** Regions in which the spalling explicitly was considered in additional simulations for scenarios without fire protection.

MN/m$^3$). No additional soil settlements or concrete primary creep were included in the simulations.

A summary of the numerical analyses carried out in this study is presented in Table 3. Hereinafter, the three tests are designated as scenarios A, B and C. In total, 15 numerical models were carried out to compare the influence of the numerical approaches. For scenarios B and C, additional numerical simulations were included to investigate the influence of concrete spalling on the tunnel behaviour. In this study, the spalling is modelled through a spalling rate of 2.5 mm/min and assuming that the spalling starting temperature is 740 °C based on the approach proposed by [41]. The mentioned spalling rate was applied in a 60 mm layer at the ceiling and lateral walls, as illustrated in Fig. 3. This height was determined according to the average spalling depth measured by Dong et al. [31] using a 3D scanner. The spalling rate was achieved by modifying the thermal properties of concrete at the cover of the inner exposed face. A high value of thermal conductivity, 5 W/(m °C), and a low thermal capacity, 0.01 MJ/(m$^3$ °C) were chosen to induce a rapid increase of temperatures at the spalling region and produce a more rapid degradation of the concrete and rebar mechanical properties. It is noteworthy to mention that a comprehensive simulation of spalling should include additional phenomena (e.g., pore pressure, moisture transport), which are more suitable for a mesoscale model.

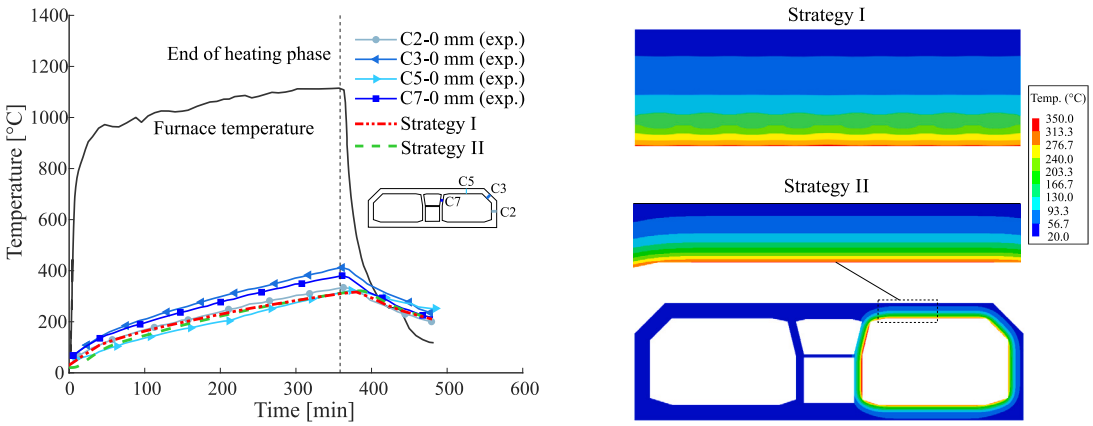


(a) Strategies I and II (b) contour plots

**Fig. 4.** Temperature evolution and contours at exposed concrete surface for fire scenario A.

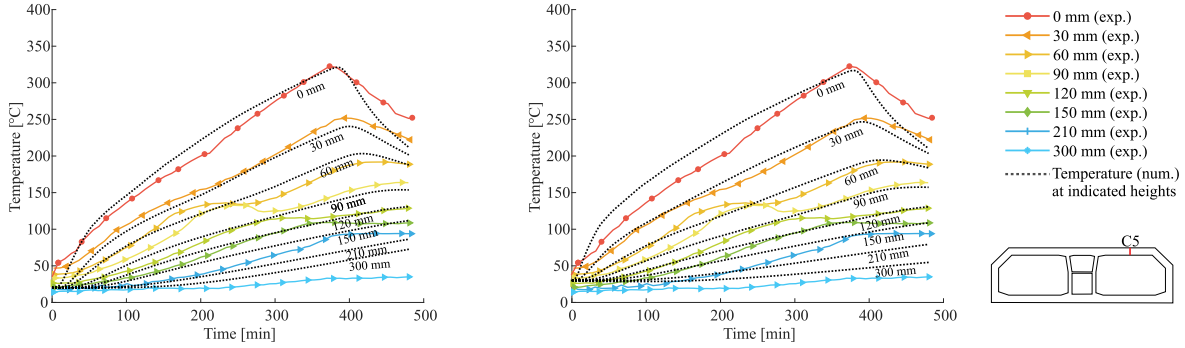


(a) Strategy I (b) Strategy II

**Fig. 5.** Temperature evolution inside concrete for fire scenario A and comparison with numerical results.

The approach proposed in this study aimed to consider the spalling effects on a macroscopic scale.

## 5. Results

### 5.1. Thermal results

Fig. 5(a) shows the temperature obtained at different locations of the exposed surface for scenario A. It can be noted that the temperature at point C5 (crown) is relatively lower than the other points. According to Duan et al. [30], this incosistency can be explained by the location of the oil burners used in the experiments. The point C5 was farther away from the flame emitted by the burners than the other gauge points. The recorded furnace temperature is also included in the plot to highlight the performance of the fire coating in reducing the temperature at the concrete cover. At the end of the heating phase, the average temperature of the fire was 1113.7 °C, and the maximum temperature of concrete was 412.4 °C. The temperature evolution obtained in both numerical strategies was similar and could represent the average temperatures reported from the experiment. Since the temperature was assumed uniform at the thermal boundary, only one curve is plotted for each strategy. Fig. 4(b) presents the temperature distribution at the tunnel ceiling cross-section obtained in Strategy I and in the full section in Strategy II. The contour plots confirm the insulation capacity of the fire coating used in the tunnel and the agreement between the considered approaches. Figure Fig. 5 shows the temperature inside the concrete, indicating a good agreement with the experimental results for both strategies.

For scenario B, the temperature at the exposed concrete surface followed the furnace temperature. In Fig. 6 and Fig. 7, the temperatures inside the concrete measured by the thermocouple RC2 are presented and compared with the numerical results. A distinction between the no spalling and explicit spalling simulation is included on the referred figures. From the experimental results, it is highligthed that the temperatures at 30 mm and 60 mm were close to the recorded at the exposed surface. As stated by Dong et al. [31], this result is explained by the spalling observed in the test. As a consequence, the concrete cover was reduced, and the thermocouples inside the concrete were not longer measuring the concrete temperature but the furncace tempearture. In addition, the temperature at the rebars was higher than 1000 °C in some regions of the heated side. From Figs. 6(b) and 7(b), it can be seen that the explicit simulation of spalling in the numerical models led to an increment of temperature as intended, whereas, the simulations in which the spalling was not considered underestimated the temperatures inside the concrete section. It is also noted that deeper within the section, concrete temperature continue to rise even after the heating phase has ended. These observations also hold for scenario C, as can be seen in Figs. 8 and 9.

Fig. 10 compares the effect of spalling through the contour plots obtained for Strategy I at the end of the heating phase of the fire scenario C. This comparison shows the increment of the heat flow at the cross-section and the exposure of the rebars to higher temperatures. As a result, a more rapid degradation of the reinforcing steel properties is induced by the fire, reducing the tunnel structural capacity.

### 5.2. Mechanical results

#### 5.2.1. Scenario A: tunnel with fire protection

The fire-resistive coating limited the damage and deformations in the tunnel segment. However, according to Duan et al. [30], cracking was observed in the unheated side of the tunnel and the mid-gallery wall. The acoustic emission sensors indicated that most of the cracks

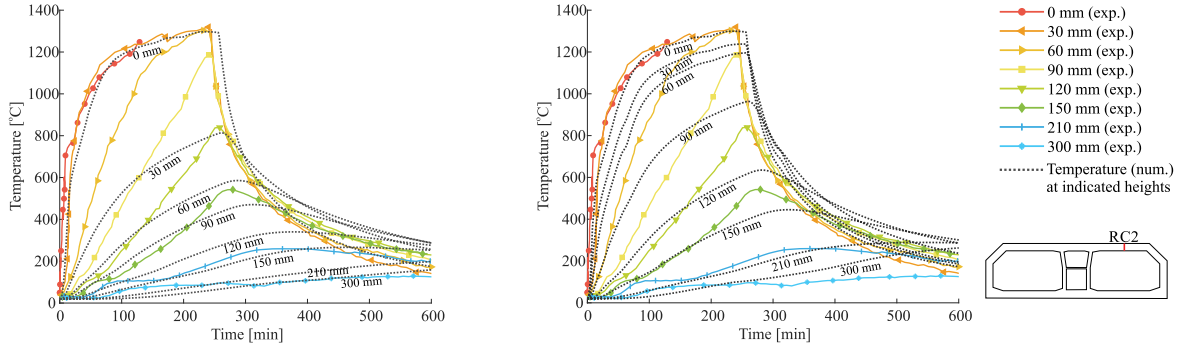


(a) No spalling (b) Explicit spalling simulation

**Fig. 6.** Temperature evolution inside concrete for fire scenario B and comparison with results of Strategy I.

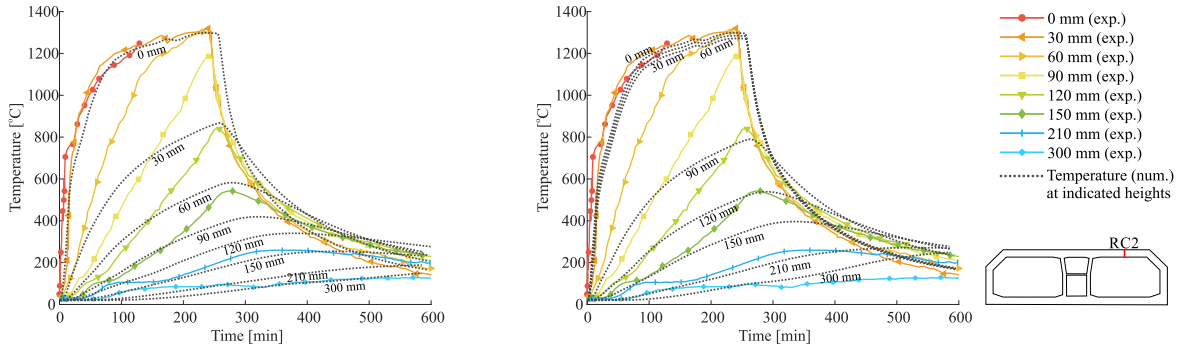


(a) No spalling (b) Explicit spalling simulation

**Fig. 7.** Temperature evolution inside concrete for fire scenario B and comparison with results of Strategy II.

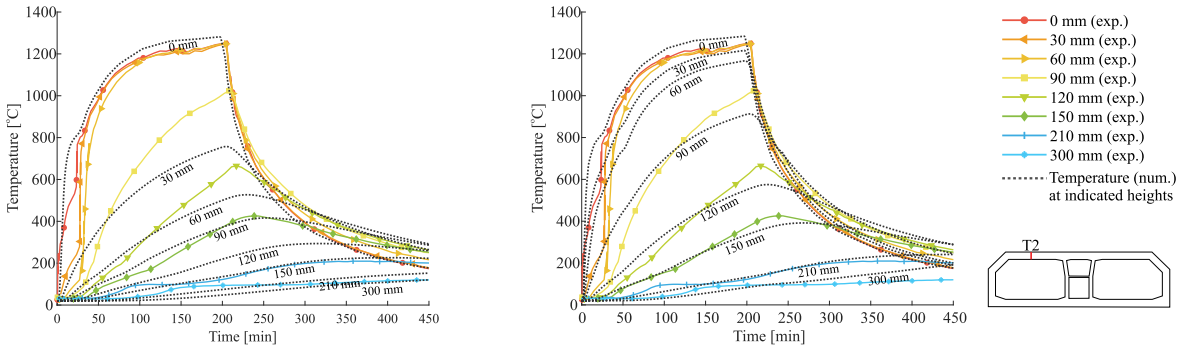


(a) No spalling (b) Explicit spalling simulation

**Fig. 8.** Temperature evolution inside concrete for fire scenario C and comparison with results of Strategy I.

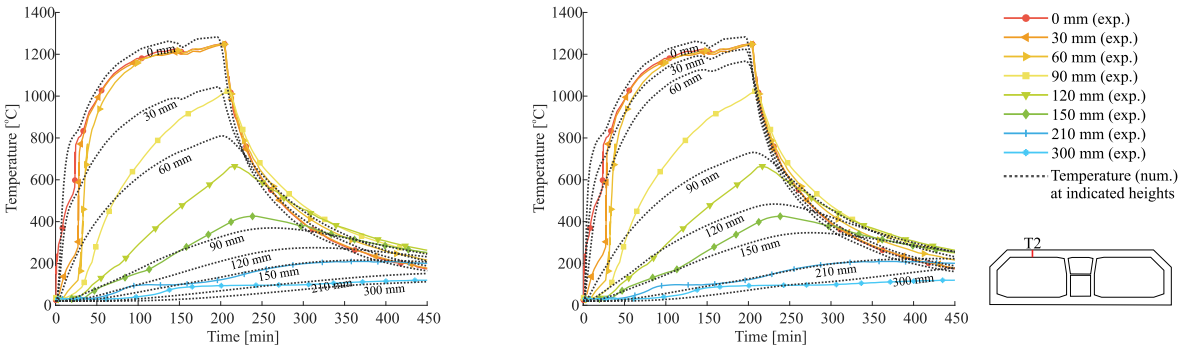


(a) No spalling (b) Explicit spalling simulation

**Fig. 9.** Temperature evolution inside concrete for fire scenario C and comparison with results of Strategy II.

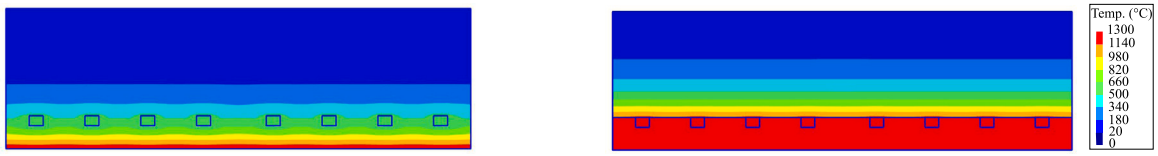


(a) No spalling (b) Explicit spalling simulation

**Fig. 10.** Contours inside concrete section for fire scenario C for Strategy I.

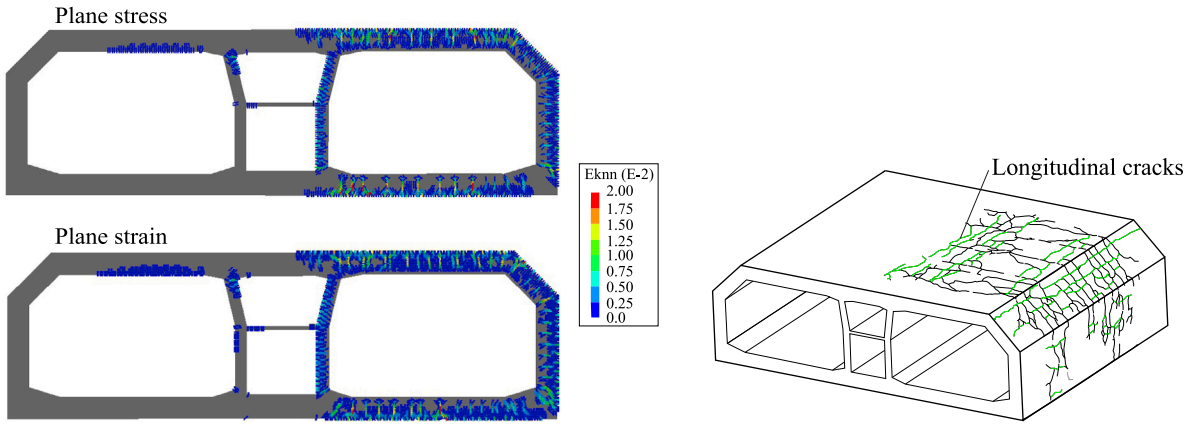


(a) (b)

**Fig. 11.** Comparison of the crack pattern obtained in the simulation and the experimental test for fire scenario A.

formed in the early stages of the fire (within 75 min), and almost no signals were recorded after 145 min, indicating the lack of new cracks and the slow growth of the existing ones. These observations are consistent with the crack propagation obtained in the numerical models from Strategy II. Fig. 11(a) presents the crack pattern at the end of the simulation for the plane stress and strain idealisations derived from the smeared mode-I crack normal strain ($\varepsilon^{k}_{nn}$). For the element size and tensile parameters used, the ultimate crack strain at which the crack is completely softened in tension is equal to 6.23 $10^{-2}$. A representation of the crack pattern obtained in the fire test is also included in Fig. 11(b). According to Duan et al. [30], the maximum crack width at the outer side was 1.86 mm. This value is higher than typical crack width limits used in the design of immersed tunnels (0.15–0.2 mm) [42]. The numerical crack width can be estimated as $w = \varepsilon^{k}_{nn} \cdot h$, with $h = 30$ mm (mesh size). The maximum crack width obtained was 0.70 and 0.72 mm, for the plane stress and plane strain models, respectively.

The location of maximum crack width correlated well with the areas with maximum stresses at the reinforcement in the numerical analyses. As shown in Fig. 12, the model-to-model comparison indicated similar results in the rebar stresses obtained for all three analyses carried out for scenario A. The stresses at the reinforcement confirmed the development of compressive stresses at the exposed side of the tunnel and tensile stresses on the unheated side.

Fig. 13(a) displays the vertical displacement at the top right corner (LVDT V1) of the tunnel section and at the ceiling midspan (LVDT V3). The numerical models show that the right tube was expanding and deforming towards the outside of the tube during the heating phase. This result is in agreement with the deformation recorded at V1. However, none of the numerical models represents the deformation at V3 (ceiling midspan) well. This result could be attributed to the limitation of the 2D approach used in both strategies and simplifications in the loading and boundary conditions, which omit possible two-way slab behaviour that occurred at the ceiling. The bending moment at the midspan of the ceiling cross-section on the exposed and unexposed tubes is presented in Fig. 13(b). Overall, the results from Strategy I and Strategy II (both plane stress/strain representations) show the same trend. The evolution of the bending moment indicates that, even

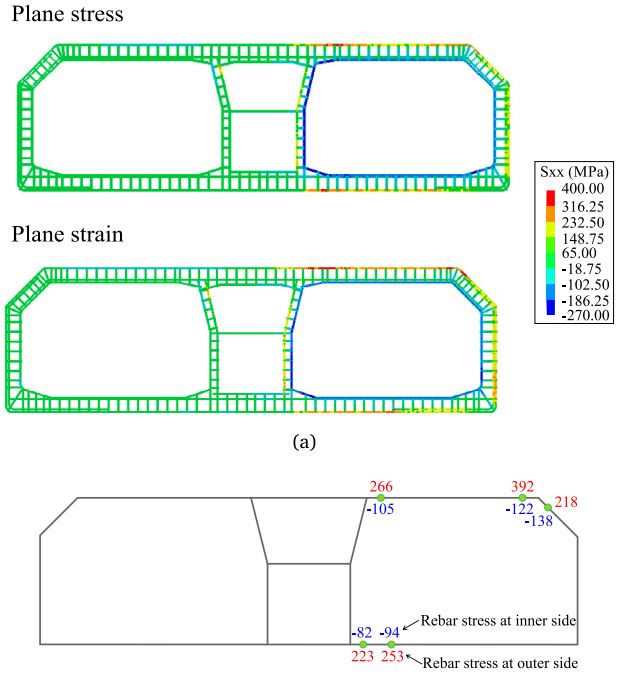


(a) (b)

**Fig. 12.** Rebar stress level for fire scenario A.

with the fire coating, the thermal gradient induces a large moment redistribution in the structure. This redistribution led to the cracking at the unheated side of the tunnel, observed in Fig. 11.

### 5.2.2. *Scenario B: tunnel with fire in both tubes*

The test under the fire scenario B demonstrated that the tunnel segment had sufficient structural capacity to withstand elevated temperatures without a full collapse. However, severe damage was reported by Dong et al. [31], including extensive concrete spalling, cracking

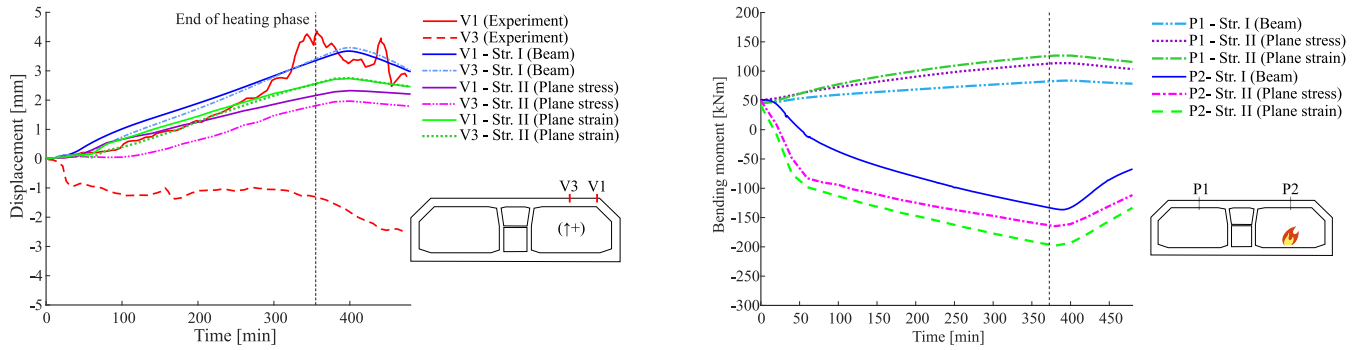


(a) Evolution of displacement

(b) Bending moments at ceiling midspan

**Fig. 13.** Mechanical response of tunnel with fire scenario A.

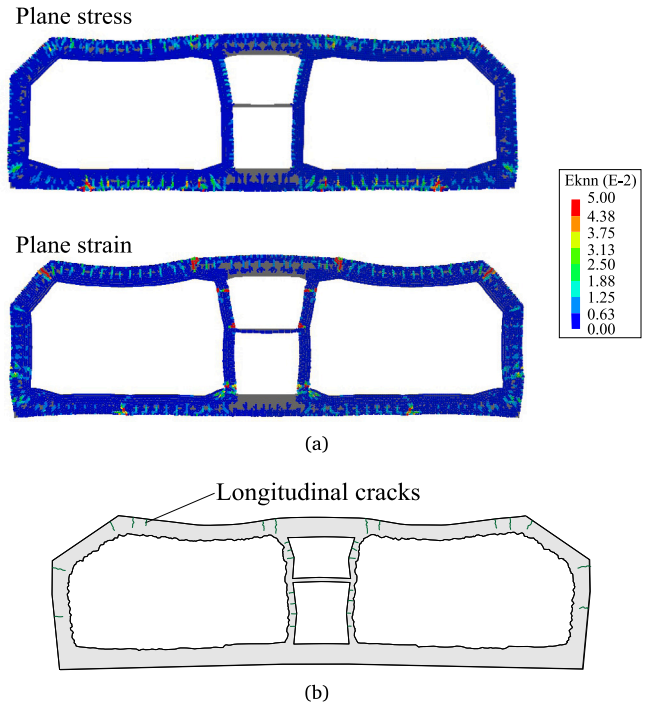


**Fig. 14.** Comparison of crack patterns obtained in the simulation and the experimental test for scenario B.

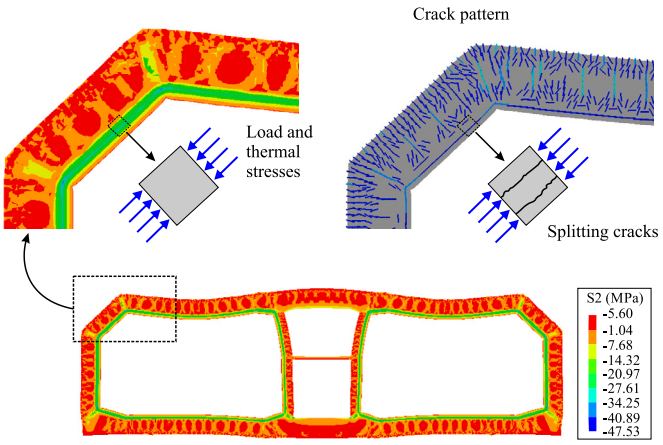


**Fig. 15.** Compressive stresses and formation of splitting cracks at cover.

on the outer side of the cross-section and melting of inner rebars exposed to fire due to spalling. Shortly after the fire test started, several cracks were observed on the outer surface of the tunnel. These cracks were mainly localised on the outer surface of the ceilings, arch and side walls. Main cracks were also detected at the corners of the ceiling and mid-walls. The locations of the main longitudinal cracks on the cross sections of the tunnel are shown in Fig. 14(b). The crack patterns at the end of the heating phase obtained in Strategy II without explicit spalling simulation are shown in Fig. 14(a) for comparison. An important aspect of the numerical crack pattern was the formation of splitting cracks at the cover, as detailed in Fig. 15. These splitting cracks were observed in models with and without explicit spalling simulation and were associated with the compressive ring action around the tunnel tubes induced by the concrete thermal expansion.

Fig. 16 compares the mechanical response with and without explicit spalling simulation. Based on the crack pattern, Dong et al. [31] concluded that the tunnel internal forces were significantly redistributed, and the negative moment near the corners increased due to the severe fire. Similar to scenario A, the corners deformed towards the outside of the section during the heating phase. This behaviour was represented by the numerical models as shown in Fig. 16(a) (refer to LVDT RV1). During the cooling phase, the experimental deformation at RV1 decreases rapidly, while the displacement from Strategy I continues to increase. The displacement from Strategy II is relatively stable during the cooling phase. More scatter was found between the numerical models and the experimental vertical displacement at the ceiling midspan (RV3). Fig. 16(b) indicates that a large bending moment redistribution occurred in the numerical models. In the case of the plane strain model, the bending moments ranged from 50 kNm to −260 kNm during the heating phase.

The influence of the explicit spalling simulation in the mechanical response is displayed in Fig. 17. The displacements obtained in the simulations are larger than the ones obtained in the test, indicating that the proposed uniform spalling scenario, together with the 2D approach, underestimated the robustness of the tunnel segment. As a result, the simulations from Strategy II were finished earlier due to convergence problems. The crack patterns presented in Fig. A.20 in the Appendix indicated that the rapid degradation generated by the spalling originated shear cracks at the corners of the tunnel cross-section that reduced the fire time resistance in the analyses. In the case of Strategy I, the analysis converged until the end of the fire. However, it is important to mention that the beam elements used in Strategy I cannot properly represent shear failure modes. To determine the fire resistance, a more detailed assessment of the shear forces obtained in the simulation is required. This limitation may also result in the large moment redistribution observed during the cooling phase in Fig. 17(b).

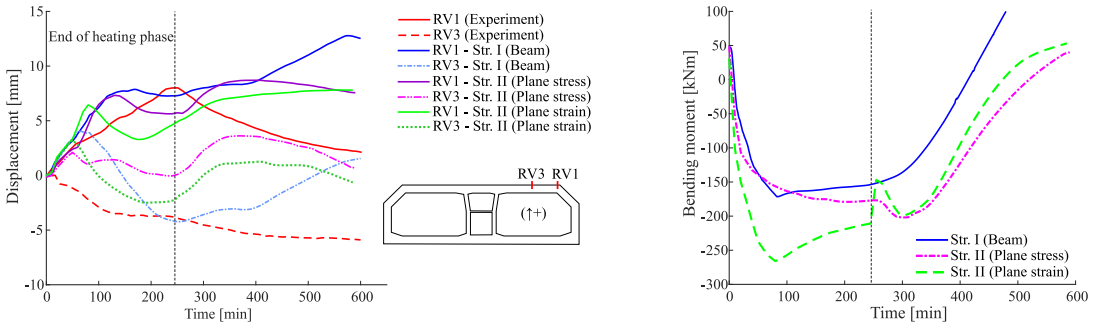


(a) Evolution of displacement (b) Bending moments at ceiling midspan

**Fig. 16.** Mechanical response tunnel with fire scenario B without explicit spalling simulation.

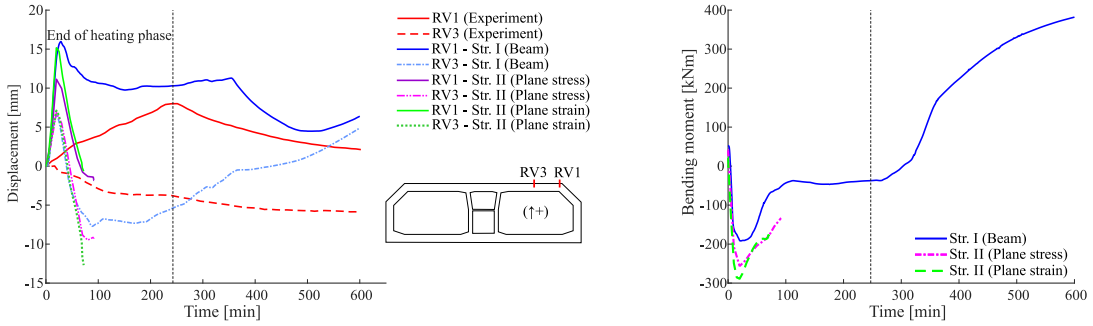


(a) Evolution of displacement (b) Bending moment at ceiling midspan

**Fig. 17.** Mechanical response tunnel with fire scenario B with explicit spalling simulation.

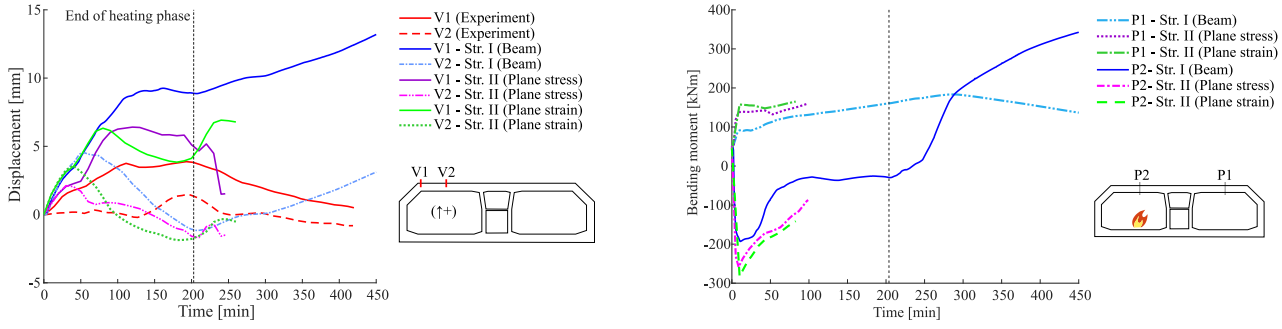


(a) Evolution of displacement (b) Bending moments at roof midspan

**Fig. 18.** Mechanical response tunnel with fire scenario C with no spalling simulation.

### *5.2.3. Scenario C: tunnel with fire in one tube*

The results of the single tube fire tunnel test showed a similar level of damage to the described in Scenario B. During the heating phase, Lin et al. [32] described that concrete spalling reduced the cross-sectional height of the cross-sectional walls, affecting the temperature distribution and reducing the capacity of the tunnel. Despite the severe damage, the tunnel did not collapse during the fire. In addition, the results showed that both the deformation and cracking of the tube exposed to the fire influenced the unexposed tube. The crack patterns obtained in the numerical models are displayed in Fig. A.21 in Appendix. Figs. 18 and 19 summarise the mechanical response of Scenario C. Overall, the results were similar to the ones discussed in the previous fire scenario. It can be observed from Figs. 18(b) and 19(b) that models with and without explicit spalling representation for Strategy II underestimated the fire time resistance. This underestimation is attributed to the development of shear cracks and the limited capacity of the 2D approach to represent the redistribution of internal forces and robustness of the real tunnel segment.

## 6. Discussion

Numerical strategies applicable to nonlinear analysis of RC tunnels exposed to fire are studied in the present paper. The simulations of three different fire scenarios reveal that both strategies detailed in Table 2 can represent the global behaviour observed in the experimental tests. However, some limitations and advantages are noted depending on the modelling choices used in the numerical models. Table 4 summarises the most important aspects of each strategy.

When comparing the two solutions, one significant difference is the representation of damage in the numerical models. In Strategy I, the damage can be investigated in the result post-processing by examining the evolution of strains and stresses at each fibre. Extensive regions where the yield strength is reached at the rebar may indicate the formation of plastic hinges, which can be used as damage indicator . In the case of Strategy II, the tunnel cross-section damage can also be investigated in terms of crack width and propagation. Both strategies point out the development of damage on the unheated side, even for

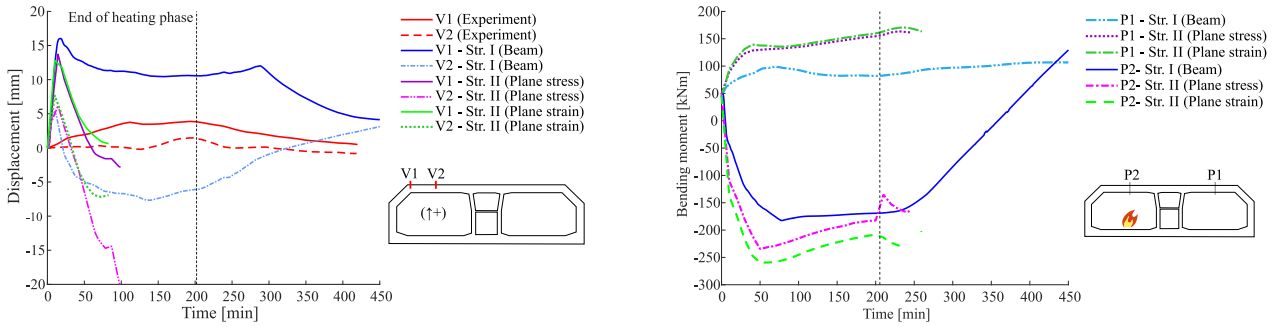


(a) Evolution of displacement

(b) Bending moments at ceiling midspan

**Fig. 19.** Mechanical response tunnel with fire scenario C with explicit spalling simulation.

**Table 4**
Summary of advantages and limitations of each strategy.

| | Strategy I | Strategy II |
|---|---|---|
| Advantages | -Few parameters are required for the input<br>-Can capture the formation of plastic hinges<br>-Explicit model for transient creep and additional concrete damage during cooling phase | -Explicit consideration of nonlinear phenomena such as cracking and confinement in compression<br>-Possibility of representing shear failure modes<br>-Continuum elements allow a better representation of in-plane stress redistribution |
| Limitations | -Cracking and shear failure cannot be explicitly represented<br>-Uniaxial material laws cannot represent possible confinement in concrete | -More parameters are required for the input<br>-Full recovery of thermal strain during the cooling phase (unrealistic behaviour) |

scenario A, in which fire protection was used. The formation of cracks on the outer side of the tunnels has important implications for the service life and reparability of tunnels. As mentioned by Nieman [11] and Van Aken [13], this phenomenon is explained by the thermal gradient over the thickness, which can only be accommodated by the bending of the walls and ceiling.

The constitutive material model in Strategy II cannot represent additional concrete degradation during the cooling phase or the residual strains in concrete due to thermal expansion and transient creep. This has important consequences in the assessment of the remaining capacity of structures exposed to fire. The assessment of this aspect in the model-to-model comparison is limited due to the relatively short cooling phase in the fire tests considered in this study. In further work, the effect of the transient creep and the concrete properties during cooling should be addressed.

The model-to-experiment comparison highlights the limitations of both strategies in representing the displacements for all three fire scenarios. The difference between the numerical and experimental results can be justified by the simplified 2D approach adopted in this study. As an alternative, 3D numerical models can be implemented in the future to investigate the tunnel deformations and robustness further. 3D shell elements (as implemented by Hua et al. [15]) are suggested to reduce the computation time.

## 7. Conclusions

This study investigate the thermo-mechanical behaviour of reinforced concrete tunnels under fire using two main numerical strategies based on NLFEA. The main differences in the proposed strategies are the finite element type and the concrete constitutive model formulations. The modelling strategies are used to investigate additional aspects, including the influence of fire protective coating and explicit spalling simulation. The assessment of these parameters is conducted through the simulation of recent experimental tests reported in the literature. The following conclusions are made:

1. The thermal analysis results obtained from the strategies predicted a similar temperature distribution in the tunnel cross-section. For scenario A, the thermal analyses confirmed the insulation properties of the fire coating and the reduction in concrete temperatures compared with the furnace temperature. For scenarios B and C, the thermal analyses indicated that the temperature distribution inside the concrete can drastically change if spalling occurs. As a consequence, the temperature of the rebars can be underestimated when the spalling is not included in the simulation of unprotected concrete exposed to severe fire scenarios.
2. The mechanical response obtained in the models was highly dependent on the spalling scenario. The assumption of a uniform spalling rate at the ceiling and the lateral walls increased rapidly the moment redistribution in the numerical response. In the case of Strategy II, the models ended during the heating phase due to convergence issues, underestimating the fire resistance of the tunnel segment.
3. The model-to-model comparison showed that using beam elements with a plastic damage model implemented in SAFIR and using 2D continuum elements with a smeared crack model in DIANA can provide a similar mechanical response. The numerical models without an explicit spalling simulation presented similar results in terms of displacements, rebar stresses, and bending moment redistribution for the three scenarios. Significant damage was observed in the unheated side of the tunnel for all three scenarios, implying serious concerns about the service life of the tunnel after a severe fire event.
4. The approach proposed in Strategy II reasonably represented the crack propagation described in the fire tests. The crack patterns obtained with plane stress and plane strain idealisations were similar for all three scenarios. The crack patterns also captured the formation of splitting cracks at the concrete cover, even in the simulations without explicit spalling. The formation of these cracks was explained by the large compressive stresses induced by the thermal gradient at the tunnel cross-section.

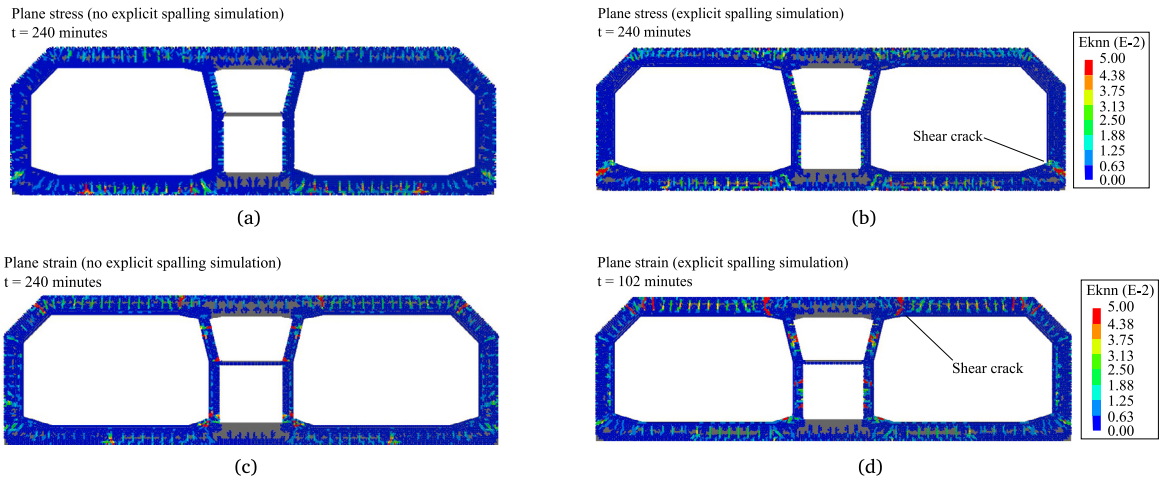


**Fig. A.20.** Crack patterns for scenario B with and without explicit spalling simulation and both plane stress/strain representations used in Strategy II.

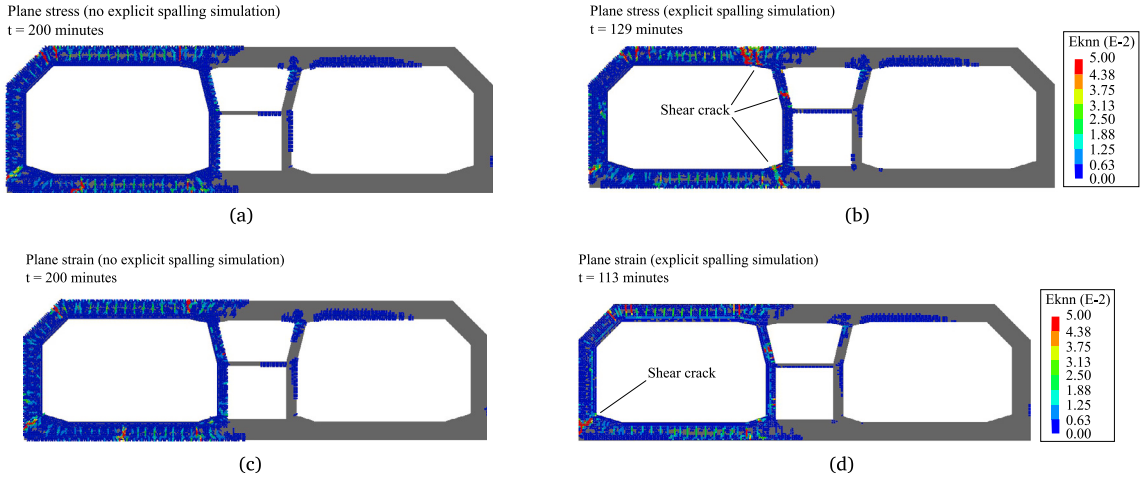


**Fig. A.21.** Crack patterns for scenario C with and without explicit spalling simulation and both plane stress/strain representations used in Strategy II.

5. The model-to-experiment comparison revealed a good agreement with the experimentally observed temperatures and damage patterns, but a significant difference in the displacement predicted by the numerical models and the one obtained in the tests. The deficient representation could be attributed to the simplified 2D approach adopted in both strategies, which omits two-way slab behaviour at the midspan ceiling and the load distribution in the tunnel longitudinal direction.

Finally, it can be concluded that the strategies developed in this paper can be used to study the global thermo-mechanical behaviour of tunnels exposed to fire. From an engineering point of view, Strategy I is appealing because it is based on simple beam elements, and its constitutive material model requires fewer input parameters. On the other hand, Strategy II can be used to investigate the crack pattern and potential shear failure modes further, but it requires more expertise in the definition of the input parameters. Future works should focus on the assessment of constitutive models of concrete properties during the cooling phase and the evaluation of the residual structural capacity after a fire event using nonlinear analysis. This further research will be helpful for the wider use of NLFEA for research and design applications of RC structures exposed to fire.

## CRediT authorship contribution statement

**Rafael Sanabria Díaz:** Writing – original draft, Software, Methodology, Formal analysis, Data curation. **Eva Lantsoght:** Writing – review & editing, Supervision, Funding acquisition, Conceptualization. **Max A.N. Hendriks:** Writing – review & editing, Validation, Funding acquisition, Conceptualization.

## Declaration of competing interest

The authors declare the following financial interests/personal relationships which may be considered as potential competing interests: Rafael Sanabria Diaz reports financial support was provided by Rijkswaterstaat (Dutch Ministry of Infrastructure and Water Management). If there are other authors, they declare that they have no known competing financial interests or personal relationships that could have appeared to influence the work reported in this paper.

## Acknowledgements

This study was supported by Rijkswaterstaat (Dutch Ministry of Infrastructure and Water Management), The Netherlands through the research project *"Brandwerendheid Landtunnels"*. The authors gratefully acknowledge this support.

## Appendix. Additional numerical crack patterns

See Figs. A.20 and A.21.

## Data availability

The data that support the findings of this study are openly available in https://gitlab.tudelft.nl/rsanabriadiaz/brandwerendheid-landtunnels.

## References


[1] C.L. Lin, C.F. Chien, Lessons learned from critical accidental fires in tunnels, Tunn. Undergr. Space Technol. 113 (2021) 103944.
[2] N. Hua, A. Tessari, N. Elhami-Khorasani, E. Mehryaar, B. Goncalves da Silva, et al., Fire in Tunnel Collaborative Project, Tech. rep., Rutgers University. Center for Advanced Infrastructure and Transportation, 2021.
[3] EN 1992-1-2, Eurocode 2: Design of Concrete Structures Part 1-2: General Rules - Structural Fire, CEN, 2004.
[4] T. Gernay, Performance-based design for structures in fire: Advances, challenges, and perspectives, Fire Saf. J. (2023) 104036.
[5] B.B.G. Lottman, The Spalling Mechanism of Fire Exposed Concrete (Ph.D. thesis), Delft University of Technology, 2017.
[6] Y. Li, E.-H. Yang, A. Zhou, T. Liu, Pore pressure build-up and explosive spalling in concrete at elevated temperature: A review, Constr. Build. Mater. 284 (2021) 122818.
[7] T. Van der Waart van Gulik, A. Breunese, R. Jansson, L. Boström, E. Annerel, Spalling behaviour of a non-spalling qualified concrete, in: 4th International Workshop on Concrete Spalling Due To Fire Exposure, October 8-9, 2015, Leipzig, Germany, 2015.
[8] R. Van Coile, B. Jovanović, R.K. Chaudhary, X. Deckers, A. Lucherini, Simplified modelling of the performance of concrete tunnels during fire and post-fire damage classification, Acta Polytech. CTU Proc. 36 (2022) 253–260.
[9] N. Hua, A. Tessari, N.E. Khorasani, The effect of geologic conditions on the fire behavior of tunnels considering soil-structure interaction, Tunn. Undergr. Space Technol. 122 (2022) 104380.
[10] T. Thienpont, F. Put, B. Jovanović, R.K. Chaudhary, R. Van Coile, Numerical investigation of the structural fire response of tunnel structures with rectangular cross-sections, in: 13th International Conference on Structures in Fire, 2024, pp. 925–935.
[11] B. Nieman, Cracking on the Unheated Side During a Fire in an Immersed Tunnel, Delft Techical University, 2008.
[12] L. Noordijk, P. Scholten, A. Breunese, C. Both, Emerging problem for immersed tunnels: fire induced concrete cracking, in: 4th International Symposium on Tunnel Safety and Security, 2010, pp. 211–222.
[13] S. Van Aken, Cracking at the Unheated Side of a Tunnel During the Heating and Cooling Phase of a Fire, Delft Techical University, 2012.
[14] P. Bernardi, E. Michelini, A. Sirico, S. Rainieri, C. Corradi, Simulation methodology for the assessment of the structural safety of concrete tunnel linings based on CFD fire–FE thermo-mechanical analysis: a case study, Eng. Struct. 225 (2020) 111193.
[15] N. Hua, N.E. Khorasani, A. Tessari, Numerical modeling of the fire behavior of reinforced concrete tunnel slabs during heating and cooling, Eng. Struct. 258 (2022) 114135.
[16] J. Cervenka, J. Surovec, P. Kabele, T. Zimmerman, A. Strauss, K. Bergmeister, Numerical simulation of fracture and damage in RC structures due to fire, Fract. Mech. Concr. Concr. Struct. 2 (2006) 727–735.
[17] P.R. Prakash, B. Pulatsu, P.B. Lourenço, M. Azenha, J.M. Pereira, A meso-scale discrete element method framework to simulate thermo-mechanical failure of concrete subjected to elevated temperatures, Eng. Fract. Mech. 239 (2020) 107269.
[18] R. Zhang, L. Jin, X. Du, Three-dimensional meso-scale modelling of failure of steel fiber reinforced concrete at room and elevated temperatures, Constr. Build. Mater. 278 (2021) 122368.
[19] R. de Borst, P.P. Peeters, Analysis of concrete structures under thermal loading, Comput. Methods Appl. Mech. Engrg. 77 (3) (1989) 293–310.
[20] E. Annerel, L. Taerwe, B. Merci, D. Jansen, P. Bamonte, R. Felicetti, Thermo-mechanical analysis of an underground car park structure exposed to fire, Fire Saf. J. 57 (2013) 96–106.
[21] J. Ožbolt, J. Bošnjak, G. Periškić, A. Sharma, 3D numerical analysis of reinforced concrete beams exposed to elevated temperature, Eng. Struct. 58 (2014) 166–174.
[22] T. Gernay, J.-M. Franssen, A plastic-damage model for concrete in fire: Applications in structural fire engineering, Fire Saf. J. 71 (2015) 268–278.
[23] V. Kodur, A. Agrawal, An approach for evaluating residual capacity of reinforced concrete beams exposed to fire, Eng. Struct. 110 (2016) 293–306.
[24] Y. Shen, H. Zhu, Z. Yan, L. Zhou, T. Zhang, Y. Men, Y. Lu, Thermo-mechanical analysis of fire effects on the structural performance of shield tunnels, Tunn. Undergr. Space Technol. 132 (2023) 104885.
[25] L. Li, J. Purkiss, Stress–strain constitutive equations of concrete material at elevated temperatures, Fire Saf. J. 40 (7) (2005) 669–686.
[26] U. Schneider, Concrete at high temperatures—a general review, Fire Saf. J. 13 (1) (1988) 55–68.
[27] Y. Anderberg, S. Thelandersson, Stress and Deformation Characteristics of Concrete at High Temperatures. 2. Experimental Investigation and Material Behaviour Model, Lund institute of technology, 1976.
[28] G. Torelli, P. Mandal, M. Gillie, V.-X. Tran, Concrete strains under transient thermal conditions: A state-of-the-art review, Eng. Struct. 127 (2016) 172–188.
[29] T. Gernay, J.-M. Franssen, A formulation of the eurocode 2 concrete model at elevated temperature that includes an explicit term for transient creep, Fire Saf. J. 51 (2012) 1–9.
[30] J. Duan, Y. Dong, J. Xiao, D. Zhang, W. Zheng, S. Zhang, A large-scale fire test of an immersed tunnel under the protection of fire resistive coating, Tunn. Undergr. Space Technol. 111 (2021) 103844.
[31] Y. Dong, J. Duan, D. Zhang, J. Liu, S. Zhu, J. Qi, Experimental research on fire resistance of the reduced scale immersed tunnel with fire in both traffic tubes, Tunn. Undergr. Space Technol. 132 (2023) 104922.
[32] J. Lin, Y. Dong, J. Duan, D. Zhang, W. Zheng, Experiment on single-tunnel fire in concrete immersed tunnels, Tunn. Undergr. Space Technol. 116 (2021) 104059.
[33] J.-M. Franssen, T. Gernay, User's manual for SAFIR A computer program for analysis of structures subjected to fire, 2022.
[34] DIANA FEA, DIANA Finite Element Analysis User's Manual Release 10.8 (Edited by Denise Ferreira), Delft, The Netherlands, 2023.
[35] D. Hordijk, Local Approach to Fracture of Concrete (Ph.D. thesis), Doctoral Thesis. Delft University of Technology, Delft, The Netherlands, 1991.
[36] P.H. Feenstra, Computational Aspects of Biaxial Stress in Plain and Reinforced Concrete (Ph.D. thesis), TU Delft, Delft University of Technology, 1993.
[37] R. Selby, F. Vecchio, A constitutive model for analysis of reinforced concrete solids, Can. J. Civil Eng. 24 (3) (1997) 460–470.
[38] F.J. Vecchio, M.P. Collins, Compression response of cracked reinforced concrete, J. Struct. Eng. 119 (12) (1993) 3590–3610.
[39] EN 1994-1-2, Eurocode 4: Design of Composite Steel and Concrete Structures – Part 1-2: General Rules - Structural Fire Design, CEN, 2005.
[40] EN 1991-1-2, Eurocode 1: actions on structures - part 1-2: general actions - actions on structures exposed to fire, CEN, 2004.
[41] N. Hua, A. Tessari, N.E. Khorasani, Characterizing damage to a concrete liner during a tunnel fire, Tunn. Undergr. Space Technol. 109 (2021) 103761.
[42] R. Lunniss, J. Baber, Immersed Tunnels, CRC Press, 2013.